Arabian Journal of Chemistry (2022) **15**, 103643

King Saud University

Arabian Journal of Chemistry

www.ksu.edu.sa
www.sciencedirect.com

ORIGINAL ARTICLE

A covalent organic framework (COF)-MnO_2 based dual signal sensing platform for sensitive alkaline phosphatase activity detection via dynamic regulating the mimicking oxidase content

Yulong Xu [a], Yanna Lin [a], Yanzhi Xing [a], Ning Chu [b,*], Xuwei Chen [a,*]

[a] *Research Center for Analytical Sciences, Department of Chemistry, College of Sciences, Northeastern University, Box 332, Shenyang 110819, China*
[b] *Bayuquan Customs District of the People's Republic of China, Yingkou 115007, China*

Received 20 October 2021; accepted 13 December 2021
Available online 17 December 2021

KEYWORDS

MnO_2 nanosheets;
Covalent organic frameworks;
Alkaline phosphatase;
Fluorescence;
Colorimetry

Abstract It is of great significance to accurately monitor the alkaline phosphatase (ALP) level as it plays an important role in living body activities. Herein, we develop a COF- MnO_2 system for ALP activity detection via the dynamic regulating the MnO_2 nanosheets content. MnO_2 nanosheets with oxidase-mimicking property can oxide the colorless 3,3′,5,5′-Tetramethylbenzidine (TMB) into blue oxidized TMB (oxTMB). The hexagonal structure and ordered mesoporous channels of DMTP-TAPB COF provide excellent space to accommodate the product oxTMB. The confinement of the dye molecules into COF structure leads to enhance color change and obvious fluorescence quench of the sensing system. The fluorescence quenching and color change dependent on the ALP level as it can dynamic regulate the MnO_2 content via the enzymatic hydrolysis of ascorbate-2-phosphate. Therefore, a COF-MnO_2 based dual signal sensing platform is successfully constructed to detect ALP activity, giving detection limit of 0.11 U L^{-1} and 0.23 U L^{-1} for fluorescence and colorimetric procedures, respectively. The practical application of the designed sensing platform is verified through the detection of ALP activity in serum samples, and satisfactory results are obtained.

* Corresponding authors.
E-mail addresses: n_chu2009@sina.com (N. Chu), chenxuwei@mail.neu.edu.cn (X. Chen).

Peer review under responsibility of King Saud University.

ELSEVIER Production and hosting by Elsevier

1. Introduction

ALP, a zinc glycoprotein made of 449 amino acids, is a key hydrolase for the phosphate metabolism of biomolecules such as protein and nucleic acid, and widely distributed in human blood and tissues (Park et al., 2018; Sepehri and Sarrafzadeh, 2018; Arabi et al., 2021). The ALP normal level

https://doi.org/10.1016/j.arabjc.2021.103643
1878-5352

is of 46–190 U L^{-1} in adult human serum (Liu et al., 2021), and the abnormal expression of ALP may indicate many diseases, such as liver cancer, diabetes mellitus, Alzheimer's disease (Siller and Whyte, 2018; Dong et al., 2017; Choi et al., 2007) and so on. Thus, it is of great significance to achieve an accurate evaluation of ALP expression. Up to date, various methodologies have been developed for the quantitative assay of ALP level, including colorimetry (Hayat et al., 2014), fluorimetry (Freeman et al., 2010), electrochemistry (Ino et al., 2012), and surface-enhanced Raman scattering (Chen et al., 2013; Arabi et al., 2021). Among these methodologies, colorimetry and fluorimetry have been gain the most popularity relying on the advantages of operating simplicity, observation by naked eyes, excellent sensitivity, and good flexibility (Wu et al., 2018; Hou et al., 2018; Li et al., 2013). Although their unique advantages, the single signal strategy has been proved to be not suitable for sensitive detection of ALP level in complex samples due to the present of potential interference. Recently, some works have been focused on the fabrication of a dual signal sensing platform for ALP detection (Yang et al., 2020; Yang et al., 2020). The dual signal strategy not only shows the advantages of colorimetry and fluorometry, but also can avoid the issues with interference and fluctuation in a complex environment, making the detection results more accurate (Han et al., 2020; Niu et al., 2019; Kim et al., 2018). However, most reported dual signal sensing platforms are poor in ingenuity and flexibility, attributing to the fact that the two detection procedures are usually fulfilled in independent reacting circles and involving their individual reagents. Therefore, it is a huge challenge to construct a dual signal sensing system of simple, low-cost, high accuracy, and rapid operation.

Covalent organic framework (COF) is a kind of highly crystalline material, and has been attracting particular attention due to their outstanding merits of high thermochemical stability, controllable chemical and physical properties, low skeleton density, and permanently open pore structure (Ding and Wang, 2013). A large number of COFs material have been synthesized over the past few years and gained extensive applications in the fields of gas storage (Mahdy et al., 2018), drug delivery (Fang et al., 2015), and heterogeneous catalysis (Wang et al., 2015) due to their high porosity, large π-conjugate system, and highly symmetric spatial rigid structure. Liu et al. synthesized a COF-JLU5 for efficient photocatalyst for oxidative C-H functionalization, and demonstrated that the large π-conjugate system of COF material contributed greatly to the improvement on charge transfer efficiency (Zhi et al., 2017). Wang et al. reported the synthesis of 2D porphyrin-based COF via the Knoevenagel condensation of 5,10,15,20-tetrakis (4-benzaldehyde) porphyrin and 1,4-phenylenediacetonitrile. The large π-conjugated of this COF led to a more effective way to transmit π-conjugation across the two-dimensional lattice and thus enhanced the electron delocalization (Ding et al., 2016). Aurelio et al. prepared a 2D COF material by using 2, 3, 10, 11, 18, 19-hexahydroxycata-hexaben coronene and pyrene-2,7-diboronic acid as precursors. The obtained COF exhibited highly crystalline with a wavy honeycomb lattice due to its highly symmetric spatial rigid structure (Martinez Abadia et al., 2019). Theoretically, the characteristic large π-conjugate system and the highly symmetric spatial rigid structure may make COFs a promising fluorescent material. While quite a few insights have been conducted on the exploration of the fluorescence property of COFs up to now.

MnO_2 nanosheet is a graphene-like two-dimensional material characterized with high catalytic activity and large surface area. As an artificial enzyme, MnO_2 nanosheet can directly catalyze substrate to produce color or fluorescence signal without the presence of hydrogen peroxide (Qu et al., 2021). At the same time, MnO_2 nanosheets can be decomposed by reducing substrates due to its favorable redox activity (Fan et al., 2021). Consequently, the favorable mimicking oxidase property of MnO_2 nanosheet has gained popularity in the quantitative assay of different analytes including biomacromolecule (Gan et al., 2019; Yan et al., 2018), antibiotics (Zhang et al., 2021), and metal ions (He et al., 2018).

Herein, we rational designed and synthesized a 2D COF material via the condensation of C_2-symmetric DMTP and C_3-symmetric TAPB. The obtained DMTP-TAPB COF adopted an 'aa' stacking mode of a P_6 space group. The large π-conjugate system and highly symmetric spatial rigid structure offered the as-prepared COF favorable fluorescence behaviors with excellent resistance to photobleaching and pH stability. MnO_2 nanosheets, as a nanozyme, could directly catalyze the oxidization of colorless TMB into blue oxidized TMB (oxTMB), which were well accommodated into DMTP-TAPB COF attributed to its hexagonal structure and ordered mesoporous channels. The absorption spectrum of oxTMB was highly overlapped with the fluorescence spectra of DMTP-TAPB COF, leading to the effective fluorescence quench of this COF material via inner-filter effect (IFE). As ALP could regulate the MnO_2 content via the enzymatic hydrolysis of ascorbate-2-phosphate (AAP) to ascorbic acid (AA), the presented ALP governed the fluorescence quenching efficiency of COF and the color change of the solution. Therefore, we constructed a COF-MnO_2 based dual signal sensing platform (fluorescence and colorimetry) for the sensitive quantitative assay of ALP activity through the dynamic regulating the MnO_2 content, and demonstrated the practicability of this sensor via quantitative assay ALP activity in human serum samples.

2. Experimental section

2.1. Preparation of MnO_2 nanosheets

The synthesis of MnO_2 nanosheets was performed according to a reported method (Liao et al., 2021). Typically, 10 mL of $MnCl_2{\cdot}4H_2O$ (0.3 mol L^{-1}) and 20 mL of TMA·OH (0.6 mol L^{-1}) containing 3 wt% of H_2O_2 were immediately mixed in a 100 mL round-bottomed flask. The obtained dark brown solution was stirred vigorously in open air at room temperature for 12 h. The bulk MnO_2 was obtained after centrifugation (10000 rpm, 15 min) was washed five times with ultrapure water and methanol alternately. After drying at 50 °C. Then, 10 mg bulk of MnO_2 was dispersed in 10 mL deionized water and ultrasonically exfoliated for 120 min. The unexfoliated MnO_2 was removed through centrifuging at low speed.

2.2. Synthesis of DMTP-TAPB COF

DMTP-TAPB COF was fabricated via a hydrothermal process. Typically, TAPB (56 mg, 0.16 mmol) and DMTP

(46 mg, 0.24 mmol) were dissolved in a mixture of 1 mL of *o*-DCB, 1 mL of *n*-BuOH and 200 μL acetic acid (6 mol L^{-1}). The resultant mixture was bottled with a 10 mL Pyrex tube, frozen and degassed three times through a liquid N_2 bath. Afterward, the top of glass tube was flame-sealed. The reaction system was heated at 120 °C for 72 h. The formed precipitate was collected via centrifugation, washed three times with anhydrous THF, and subjected to Soxhlet extraction used THF as the solvent for 1 day. The powder collected was dried at 120 °C under vacuum overnight to give a yellow-colored solid.

2.3. Fluorescence and colorimetric assay of ALP activity

100 μL AAP (2 mmol L^{-1}), 100 μL ALP of different activities (0, 0.5, 1, 2, 4, 6, 8, 10, 20, 30, 40, 50, 60, 80 U L^{-1}) were mixed with 100 μL PBS buffer (1/15 mol L^{-1}, pH = 8.0). The resultant mixtures were maintained at 37 °C for 30 min. Subsequently, 50 μL MnO_2 nanosheets solution (0.4 mg mL^{-1}), 130 μL HAc-NaAc buffer (1/15 mol L^{-1}, pH = 3.5), 20 μL TMB solution and 100 μL DMTP-TAPB COF (0.5 mg mL^{-1}) were added into the mixture in sequence. The resultant solutions were incubated at 37 °C in dark for 10 min before spectral measurements. Finally, the fluorescence spectra with an excitation wavelength of 400 nm and UV–Vis absorption spectra in the wavelength range of 500–750 nm were recorded.

2.4. ALP activity assay in human serum samples

Blood samples were donated by healthy volunteers. The collected serum samples were mixed with ice acetone at the ratio of 1:4, then the mixtures were centrifuged at 4000 rpm for 15 min for protein removal. The serum was 10 - fold diluted with pH 8.0 PBS buffer and then directed the fluorescence and colorimetric assay procedures. The spiked samples were prepared via adding ALP of different activities (2, 5, 10 U L^{-1}) into the diluted serum samples.

3. Results and discussion

3.1. Choice of materials

Nanozymes have been aroused great interest in research for their unique advantages of tunable catalytic activity, high stability against harsh environments, flexibility in composition and structural design, and excellent biocompatibility. The enzymatic activities of nanozyme are closely related to the size, morphology, surface modification and valence, composition, and architecture of the active sites. MnO_2 nanosheets are a kind of two-dimensional flake-like structure with a large surface area, which endows the MnO_2 nanosheets with favorable oxidase-mimicking property. As an oxidase, MnO_2 nanosheets can oxide the colorless substrate 3,3′,5,5′-Tetramethylbenzi dine (TMB) into blue oxidized TMB (oxTMB), but the presence of reducing substrates, such as ascorbic acid, will induce the reduction of MnO_2 into Mn^{2+}, resulting in the loss of oxidase-mimicking activity of MnO_2 nanosheets. COF is a kind of highly crystalline material, and the characteristic large π-conjugate system and the highly symmetric spatial rigid structure, which makes COF become a potential spectral probe in sensing applications. Moreover, the hexagonal structure and ordered 1D channels provide available space to host guest molecule, i.e., the dye TMB and oxTMB. The confinement of the dye molecules into the COF structure may pose a great effect on the spectral characteristics of enveloping guest molecule and COF itself. Therefore, the catalytic ability of MnO_2 nanosheets and the fluorescence property of COF materials are exploited to the construct a dual signal sensing system for the detection of ALP activity.

3.2. Characterizations of MnO_2 nanosheets and DMTP-TAPB COF

In present study, bulk MnO_2 was first prepared at room temperature, and then MnO_2 nanosheets were obtained via the ultrasonic exfoliation of the bulk MnO_2. TEM image revealed that the obtained MnO_2 nanosheets were of typical two-dimensional layer structure with multiple folds and crinkles (Fig. 1A). The EDS mapping indicated that the presence of Mn and O elements in MnO_2 nanosheets (Fig. S1A). The MnO_2 nanosheets characteristic functional peaks of 654.7 eV and 642.8 eV were observed in XPS spectrum (Fig. S1B). These results indicated that the MnO_2 nanosheets were successfully prepared. The COF material was prepared with the electron-rich aromatic C_3-symmetric TAPB and the electron-donating (lone pairs on the oxygen) methoxy-substituted phenyl edges of C_2-symmetric DMTP as the building blocks via a solvothermal condensation process (Scheme S1). During the [3 + 2] imine condensation reaction, the electron-rich monomer TAPB, which had three phenyl rings, was highly conjugated and offered the base for π-π interactions and electron transfer (Thomas et al., 2019), the DMTP with two electron-donating methoxy groups on each phenyl edge lose two lone pairs from the oxygen atoms over the central phenyl ring, which those structural characteristics of monomers would reinforce the interlayer interactions, stabilized the structure and facilitated the crystallization of the final favorite COF product (Xu et al., 2015). The reaction temperature plays a central role on COF preparation as it governs the initial nucleation and crystal growth (Liu et al., 2019); DMTP-TAPB COF with favorable crystallinity was readily obtained under a reaction temperature of 120 ℃ (Fig. S2). MS simulation results indicated that the obtained DMTP-TAPB COF owned a hexagonal structure with a pore size of ∼3.3 nm and ordered mesoporous 1D channels with methoxy units on the walls (Fig. S3), attributed to the [3 + 2] imine condensation reactions (Guan et al., 2020).

As shown in Fig. 1B, the SEM image revealed that DMTP-TAPB COF was with a shape of nanoflower. As shown in Fig. 1C, the C = O stretching vibrations at 1676 cm^{-1} attributed to the aldehyde group of DMTP and the N-H symmetric and asymmetric stretching vibrations at 3342 cm^{-1} ascribed to the amino group of TAPB were clearly observed. After the condensation reaction, the N-H stretching signal and C = O stretching signal disappeared in the FT - IR spectra of DMTP-TAPB COF, and a new peak centered at 1591 cm^{-1} appeared, assigned to the formed C = N bond (Zhang et al., 2017). The changes in the FT - IR spectra well indicated the occurrence of a condensation reaction between the monomers and the formation of an imine bond in the obtained DMTP-TAPB COF. The as-prepared DMTP-TAPB COF was further corroborated via the XRD diffraction assay (Fig. 1D). The

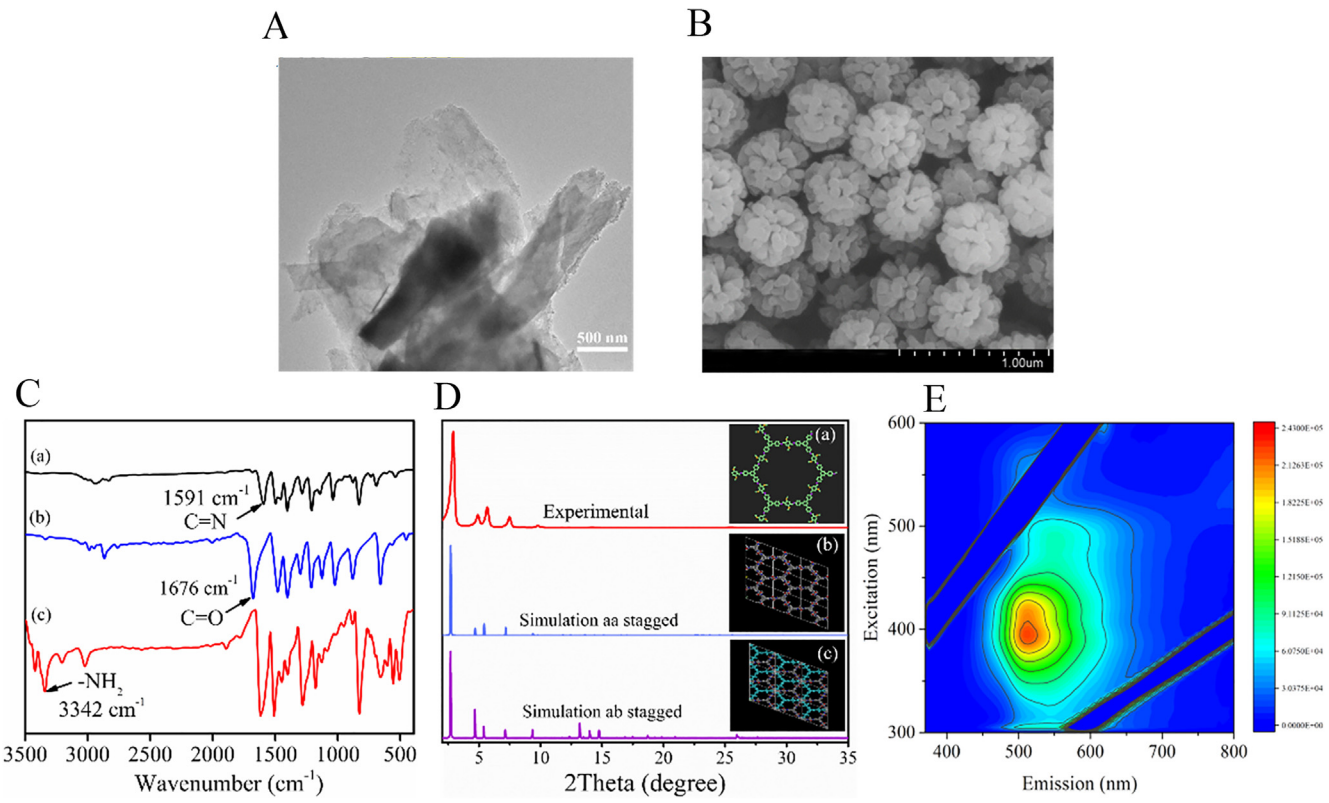

Fig. 1 (A) TEM image of MnO_2 nanosheets. (B) SEM image of DMTP-TAPB COF. (C) FT - IR spectra of (a) DMTP-TAPB COF, (b) DMTP, (c) TAPB. (D) XRD profiles of DMTP-TAPB COF of the experimentally observed (red), simulated used the aa (blue) and ab (purple) stacking modes. Insert: (a) chemical structure of DMTP-TAPB COF, unit cells of the aa (b) and ab (c) stacking modes. (E) The 3D fluorescence spectrum of DMTP-TAPB COF.

XRD diffraction pattern showed several peaks at 2θ = 2.76, 4.82, 5.60, 7.42 and 9.70, corresponding to the face of (100), (110), (200), (210) and (220) (Zhang et al., 2017); suggested that the obtained product was of high purity with favorable crystallinity. Moreover, a density-functional tight-binding method exploring Lennard-Jones dispersion was used to simulate the optimal structure of DMTP-TAPB COF. In the stacked frameworks, DMTP-TAPB COF adopted the 'aa' stacking mode of a P_6 space group with a = b = 37 Å, c = 3.5 Å, α = β = 90°, γ = 120° (Fig. S4). The TGA result indicated that nearly no weight loss was observed before the temperature reached 400 °C (Fig. S5), suggested the excellent thermo-stability of this DMTP-TAPB COF (Stegbauer et al., 2014). The BET surface area of DMTP-TAPB COF was deduced to be 3185 $m^2\ g^{-1}$ according to N_2 adsorption–desorption isotherms (Fig. S6). As shown in Fig. 1E, the optimum fluorescence excitation and emission were 400 nm and 514 nm, respectively. At the same time, the DMTP-TAPB COF exhibited favorable anti-photobleaching performance and the pH stability (Figs. S7 and S8).

3.3. The principle of COF-MnO_2 based dual signal sensing platform for ALP activity detection

The principle of this COF-MnO_2 based dual signal sensing platform for ALP activity detection was illustrated in Scheme 1. MnO_2 nanosheets were lamellated with favorable mimic-oxidase activity, which could oxide the colorless TMB into blue oxTMB (Yan et al., 2017). TMB was an aromatic dye with a two benzene rings structure, and the plane dimension of ~11.49 Å × 7.50 Å (Fig. S9), while the DMTP-TAPB COF was merited with a hexagonal cell structure with a pore size of ~3.3 nm (Fig. S3), which was much larger than the size of TMB. Therefore, TMB molecules were prone to

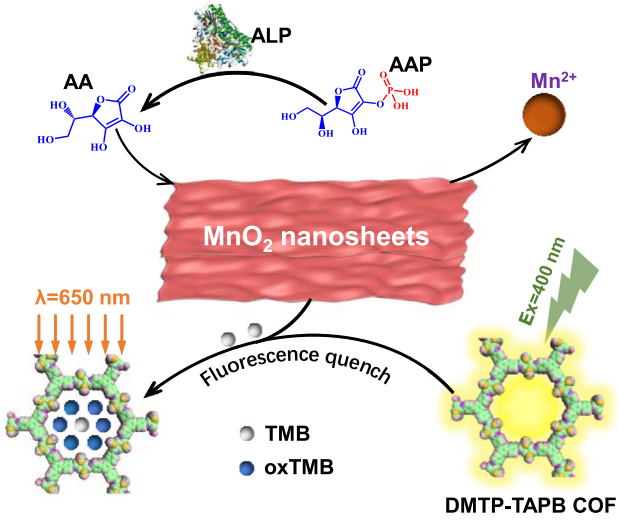

Scheme 1 Illustration for COF-MnO_2 based dual signal sensing platform for detection of ALP activity.

enter into the hexagonal cell driven by the hydrophobic and π-π reactions. That is, the DMTP-TAPB COF provided favorable space for the accommodation of TMB and oxTMB molecules (Fig. S10), and the confinement of the dye molecules enhanced the fluorescence quenching efficiency (Pachfule et al., 2018).

It was found that the UV–Vis absorption spectrum of oxTMB overlapped heavily with the excitation spectrum of DMTP-TAPB COF (Fig. 2A), which thus led to efficiently quench of DMTP-TAPB COF fluorescence. The fluorescence quench induced by spectral overlap might be attributed to the IFE or fluorescence resonance energy transfer. As shown in Fig. 2B, DMTP-TAPB COF owned a fluorescence lifetime of about 3.36 ns, and changed to 3.25 ns with the presence of oxTMB, implying that there was no electron or energy transfer taking place between oxTMB and COF material. Moreover, the presence of oxTMB did not affect the emission maximum of DMTP-TAPB COF, suggested that the fluorescence quenching of DMTP-TAPB COF by oxTMB was readily induced by IFE, rather than fluorescence resonance energy transfer (Feng et al., 2020).

AAP was an enzymatic hydrolysis substrate with an ester group and could be hydrolyzed through the breaking of ester bonds to produce AA with ALP as catalyst. AA was able to reduce MnO_2 nanosheets into Mn^{2+} (Zhang et al., 2021), the reduced MnO_2 content thus resulted in the decreased oxTMB production, and subsequent decreased fluorescence quench efficiency. It can be seen in Fig. 2C that there was peak centered at 650 nm in the UV–Vis absorption spectrum of oxTMB. Nearly no color change was observed with the presence of substrate AAP or catalyst ALP alone, while the co-presence of AAP and ALP would cause obvious color change, reflected at the clear decrease of adsorption bands. Similar phenomena were also found on the fluorescence response of this sensing system. The addition of substrate AAP or catalyst ALP alone offered no influence on the COF fluorescence, while significant fluorescence recovery was observed when AAP and ALP were simultaneously presented, attributed to the occurrence of enzymatic hydrolysis (Fig. 2D). As the presence of ALP could dynamic regulate the MnO_2 nanosheets content, which eventually governed the color change and the fluorescence quench efficiency of the COF-MnO_2 system, thus it

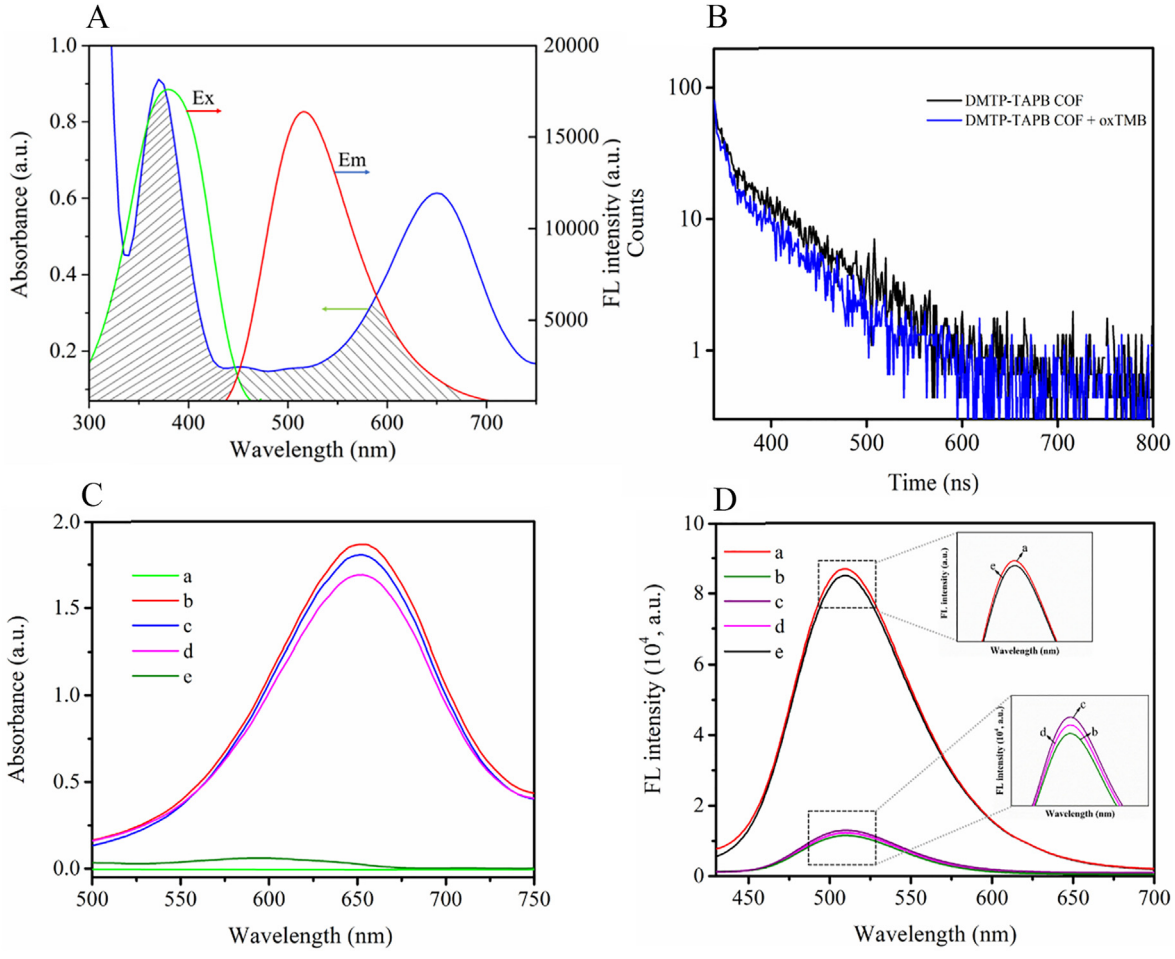

Fig. 2 (A) Excitation (λex = 400 nm, green) and emission (λem = 514 nm, red) spectrum of DMTP-TAPB COF and UV – Vis absorption spectrum of oxTMB (blue). (B) Fluorescence decay profile of DMTP-TAPB COF (black) in the presence of oxTMB (blue). (C) UV – Vis spectra of (a) TMB, (b) MnO_2 nanosheet + TMB, (c) MnO_2 nanosheet + TMB + AAP, (d) MnO_2 nanosheet + TMB + ALP and (e) MnO_2 nanosheet + TMB + AAP + ALP. (D) Fluorescence emission spectrum of DMTP-TAPB COF in the present of (a) no reactants, (b) TMB + MnO_2 nanosheet, (c) TMB + MnO_2 nanosheet + AAP, (d) TMB + MnO_2 nanosheet + ALP, (e) TMB + MnO_2 nanosheet + AAP + ALP.

was adopted to construct a dual signal sensing platform for ALP quantitative assay.

3.4. Optimization of experimental parameters

In order to obtain a high sensitivity for the proposed COF-MnO_2 based dual signal sensing system, the effect of the concentration of MnO_2 nanosheets and TMB on the signal response were investigated. As shown Fig. 3A, both the fluorescence and absorbance response increased with MnO_2 concentration up to 0.3 mg mL^{-1}, then leveled off when the concentration became higher than 0.3 mg mL^{-1}. These might be ascribed to fact that more oxTMB was produced with the increasing of MnO_2 nanosheet concentration, thus obvious fluorescence and color changes were achieved. When TMB in the sensing system was fully oxidized, the increase of MnO_2 nanosheet concentration (>0.3 mg mL^{-1}) didn't contribute to the oxTMB production, thus nearly no change on the fluorescence and absorbance response was observed. Similar response trends were also found for the TMB concentration (Fig. 3B). The TMB concentration contributed to the fluorescence and absorbance response when it was lower than 0.6 mmol L^{-1}, and the further increase of TMB concentration caused no obvious change on the signals due to the limited MnO_2 content. Therefore, a MnO_2 concentration of 0.3 mg mL^{-1} and a TMB concentration of 0.6 mmol L^{-1} were adopted for the ensuing sensing applications.

3.5. Selectivity

To evaluate the selectivity of this COF-MnO_2 based dual signal sensing platform for ALP activity, the influence of coexisting species in human serum, including NH_4^+, Na^+, K^+, Ca^{2+}, Mg^{2+}, Zn^{2+}, Cu^{2+}, tryptophan (Try), histidine (His), valine (Val), phenylalanine (Phe), leucine (Leu), glucose (Glu), proline (Pro), immunoglobulin (IgG), albumin (Alb), trypsin (Try), lysozyme (Lys), lactate dehydrogenase (LDH), butyrylcholinesterase (BuChE), thrombin (Thr), acetylcholinesterase (AChE), Cl^-, SO_4^{2-}, PO_4^{3-}, NO_3^-, CO_3^{2-}, and HCO_3^- were investigated at a concentration level of 10-fold higher than that of tested ALP to evaluate their potential interference. As shown in Fig. 4, while no obvious color change for the sensing system were observed with the addition of these coexisting species, only ALP induced clear color change from blue to pale yellow. At the same time, the significant fluorescence recovery of this COF-MnO_2 based dual signal sensing system was achieved via the presence of ALP, which was not observed for other species. These well suggested that this COF-MnO_2 based dual signal sensing platform provided a highly specific strategy for

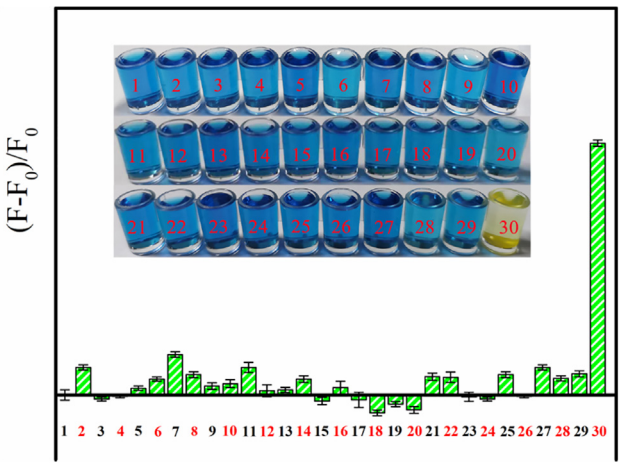

Fig. 4 The signal response of COF-MnO_2 based dual signal sensing platform for potential interferants. (1) Blank; 10 mmol L^{-1} of NH_4^+(2), Na^+(3), K^+(4), Ca^{2+}(5), Mg^{2+}(6), Zn^{2+}(7), Cu^{2+}(8), Try(9), His(10), Val(11), Phe(12), Leu(13), Glu(14) and Pro(15); 1 mg L^{-1} of IgG(16) and Alb(17), 1000 U L^{-1} of Try(18), Lys(19), LDH(20), BuChE(21), Thr(22) and AChE(23); 10 mmol L^{-1} of Cl^-(24), SO_4^{2-}(25), PO_4^{3-}(26), NO_3^-(27), CO_3^{2-}(28), HCO_3^-(29); 100 U L^{-1} of ALP(30) (F_0 and F were the fluorescent intensity of COF-MnO_2 based dual signal sensing platform at 514 nm in the absence and presence of ALP). The insets showed the photographs of the system after the addition of the corresponding species. Error bars were estimated from triplicate measurements.

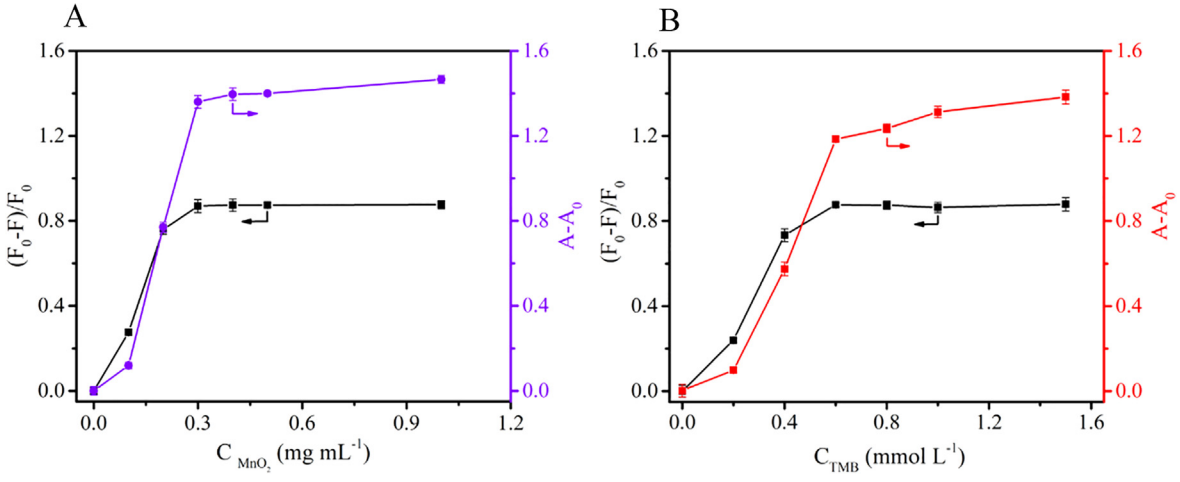

Fig. 3 Effect of different experimental parameters: (A) Concentration of MnO_2 nanosheets. (B) Concentration of TMB.

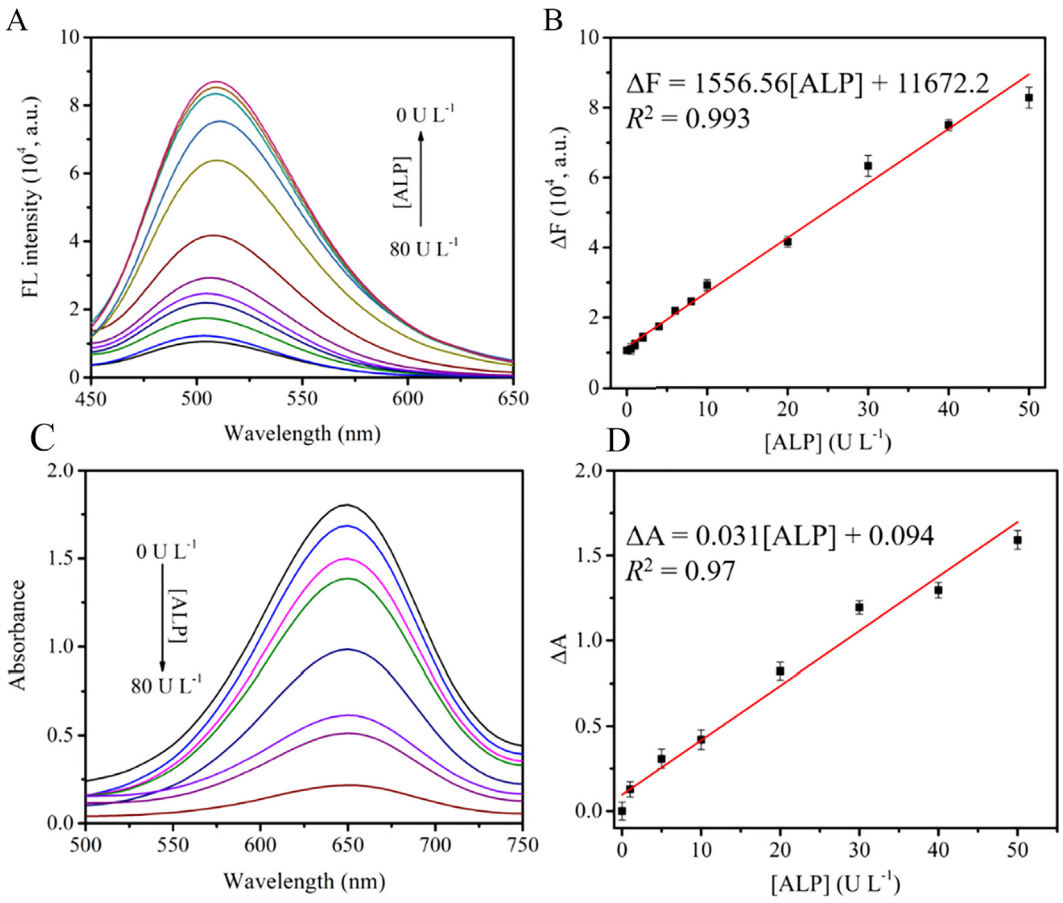

Fig. 5 (A) Fluorescence titration spectra of the sensing platform under different ALP activity. (B) The calibration relationship between the fluorescence intensity and the ALP activity. Error bars were estimated from triplicate measurements. (C) UV–Vis absorption of the sensing system to different ALP activity. (D) The calibration relationship between the absorbance and the ALP activity. Error bars were estimated from triplicate measurements.

Table 1 Comparisons of the analytical performance of sensing system for ALP activity assay.

Sensing system	Method	Linear range(U L^{-1})	LOD (U L^{-1})	Ref.
Ce (IV) ions-TMB	Colorimetry	0–50	2.3	(Song et al., 2018)
G20-Cu (II) complex	Colorimetry	20–200	0.84	(Yang et al., 2016)
Gold/silver nanorod	Colorimetry	0–120	5.4	(Shi et al., 2016)
Cu^{2+}-TMB-H_2O_2	Colorimetry	0–200	1.25	(Hu et al., 2017)
Fe (II)-phenanthroline	Colorimetry	5–100	3.3	(Hu et al., 2017)
F-PDA-MnO_2	Fluorometry	1–80	0.34	(Xiao et al., 2018)
g-C_3N_4/CoOOH	Fluorometry	1–30	0.92	(Liu et al., 2019)
DNA-AgNCs	Fluorometry	30–240	5	(Ma et al., 2016)
BSA-AuNCs	Fluorometry	1–6	0.16	(Ni et al., 2019)
MIL-53(Fe)	Fluorometry	2–80	0.7	(Ye et al., 2019)
THP[a] probe	Fluorometry	0–200	1.21	(Huang et al., 2021)
DXMP[b] probe	Fluorometry	20–200	3.8	(Pang et al., 2021)
DMTP-TAPB COF	Colorimetry	0.5–50	0.23	This work
	Fluorometry	0.5–50	0.11	

[a] 2-(benzo[d]thiazol-2-yl)-4-(1,4,5-triphenyl-1*H*-imidazole-2-yl) phenyl dihydrogen phosphate.
[b] 4-(2,2-dicyanovinyl)-2,3-dihydro-1*H*-xanthen-6-yl dihydrogen phosphate.

Table 2 Determination of ALP content in human serum samples (n = 3).

Samples	Added ($U\ L^{-1}$)	Fluorometry			Colorimetry		
		Detected ($U\ L^{-1}$)	Recovery (%)	RSD (%)	Detected ($U\ L^{-1}$)	Recovery (%)	RSD (%)
#1	2.00	2.12 ± 0.18	106.0 ± 9.0	6.58	2.04 ± 0.10	102.0 ± 5.0	4.01
	5.00	5.45 ± 0.13	109.0 ± 2.6	1.71	5.12 ± 0.08	102.4 ± 1.6	1.15
	10.00	10.85 ± 0.17	108.5 ± 1.7	0.11	10.03 ± 0.07	100.3 ± 0.7	0.51
#2	2.00	2.47 ± 0.04	123.5 ± 2.0	1.32	2.08 ± 0.08	104.0 ± 4.0	3.10
	5.00	5.61 ± 0.03	112.2 ± 0.6	0.22	5.04 ± 0.02	100.8 ± 0.4	3.24
	10.00	11.12 ± 0.03	111.2 ± 0.3	2.21	10.05 ± 0.01	100.5 ± 0.1	0.08

ALP quantitative assay, due to that fact that the presence of ALP dynamically regulates the MnO_2 nanosheets content.

3.6. Dual signal assay of ALP activity

To gain an insight into the analytical performance of this COF-MnO_2 based dual signal sensing platform towards ALP quantitative assay, the fluorescent recovering titrations with different ALP contents were conducted, and the fluorescence intensity of this platform was recorded under an excitation of 400 nm. As shown in Fig. 5A, the fluorescence of the COF-MnO_2 based dual signal sensing system was recovered in an ALP-dependent way. The fluorescence change ΔF ($\Delta F = F - F_0$, F and F_0 were the fluorescence intensity at 514 nm in the presence and absence of ALP) increased linearly with the ALP concentration ranging from 0.5 $U\ L^{-1}$ to 50 $U\ L^{-1}$. The regression equation was $\Delta F = 11672.2 + 1556.56$ [ALP] ($U\ L^{-1}$) ($R^2 = 0.993$) (Fig. 5B). The limit of quantitative assay was derived to be 0.11 $U\ L^{-1}$ according to the definition by IUPAC criteria ($3\sigma/k$, n = 11).

Meanwhile, as shown in Fig. 5C, the absorbance change ΔA ($\Delta A = A_0 - A$, A_0 and A were the absorbance at 650 nm in the absence and presence of ALP) exhibited good linear relationship with ALP activity in the range of 0.5 $U\ L^{-1}$ to 50 $U\ L^{-1}$, The regression equation was $\Delta A = 0.094 + 0.031$ [ALP] ($U\ L^{-1}$) ($R^2 = 0.97$) (Fig. 5D), with a detection limit of 0.23 $U\ L^{-1}$. Table 1 summarized the analytical performance including linear range and limit of detection (LOD) of reported fluorometric and colorimetric systems for ALP quantitative assay. As can be seen that this COF-MnO_2 based dual signal sensing method offered superiority in sensitivity compared with other systems, which might be ascribed to the strong capturing ability and confinement of DMTP-TAPB COF to dye molecules (Liu et al., 2018).

3.7. ALP activity assay in the actual sample

ALP was an indispensable clinical biomarker existing in serum. To verify the practical applicability of this dual signal sensing platform, the level of ALP in human serum samples were determined by the fluorescence and colorimetric procedures, and the method was further validated by spiking recoveries of ALP in serum samples. As shown in Table 2, the recoveries of adding ALP were in the range 106.0–123.5% (fluorescence) and 100.5%–104.0% (colorimetric), respectively. The results demonstrated the accuracy and reliability of this COF-MnO_2 based dual signal platform for ALP determination in practical applications.

4. Conclusion

We rationally designed a COF-MnO_2 based dual signal (fluorescence and colorimetry) platform for the sensitive ALP activity detection. The DMTP-TAPB COF was prepared via a simple [3 + 2] imine condensation reaction, and merited with favorable fluorescence behaviors resulted from its large π-conjugation system and symmetric spatial rigid structure. The unique hexagonal structure and ordered mesoporous channels provided the obtained COF with excellent TMB/oxTMB accommodation ability. The effective fluorescence quench caused by the IFE between COF and oxTMB, and the efficient fluorescence restoration by regulating the oxTMB production with ALP offered the base for sensitive ALP quantitative assay. At the same time, the confinement of the dye in COF structure gave the improved sensitivity for colorimetric ALP detection. The developed COF-MnO_2 based dual signal platform demonstrated its practicality by the quantitative assay of ALP content in serum samples. This research not only provides a potential path for ALP activity quantitative assay in clinical diagnosis, but also expands the applications of COFs in biological analysis by taking advantage of its unique structure and favorable fluorescence properties.

Acknowledgements

The authors appreciate financial supports from the Natural Science Foundation of China (21727811), and Fundamental Research Funds for the Central Universities, China (N2005027).

Appendix A. Supplementary material

Supplementary data to this article can be found online at https://doi.org/10.1016/j.arabjc.2021.103643.

References

Arabi, M., Ostovan, A., Li, J., Wang, X., Zhang, Z., Choo, J., Chen, L., 2021. Molecular imprinting: green perspectives and strategies. Adv. Mater. 33, 2100543–2100576.

Arabi, M., Ostovan, A., Zhang, Z., Wang, Y., Mei, R., Fu, L., Wang, X., Ma, J., Chen, L., 2021. Label-free SERS detection of raman-inactive protein biomarkers by raman reporter indicator: toward ultrasensitivity and universality. Biosens. Bioelectron. 174, 112825–112834.

Chen, Y., Cheng, H., Tram, K., Zhang, S., Zhao, Y., Han, L., Chen, Z., Huan, S., 2013. A paper-based surface-enhanced resonance

Raman spectroscopic (SERRS) immunoassay using magnetic separation and enzyme-catalyzed reaction. Analyst 138, 2624–2631.
Choi, Y., Ho, N.H., Tung, C.H., 2007. Sensing phosphatase activity by using gold nanoparticles. Angew. Chem. Int. Ed. 119, 721–723.
Ding, S., Wang, W., 2013. Covalent organic frameworks (COFs): from design to applications. Chem. Soc. Rev. 42, 548–568.
Ding, S., Dong, M., Wang, Y., Chen, Y., Wang, H., Su, C., Wang, W., 2016. Thioether-based fluorescent covalent organic framework for selective detection and facile removal of mercury (II). J. Am. Chem. Soc. 138, 3031–3037.
Dong, L., Qian, J., Hai, Z., Xu, J., Du, W., Zhong, K., Liang, G., 2017. Alkaline phosphatase-instructed self-assembly of gadolinium nanofibers for enhanced T2-weighted magnetic resonance imaging of tumor. Anal. Chem. 89, 6922–6925.
Fan, Z., Zhou, Z., Zhang, W., Zhang, X., Lin, J.M., 2021. Inkjet printing based ultra-small MnO_2 nanosheets synthesis for glutathione sensing. Talanta 225, 121989–121995.
Fang, Q., Wang, J., Gu, S., Kaspar, R.B., Zhuang, Z., Zheng, J., Guo, H., Qiu, S., Yan, Y., 2015. 3D porous crystalline polyimide covalent organic frameworks for drug delivery. J. Am. Chem. Soc. 137, 8352–8355.
Feng, S., Lv, J., Pei, F., Lv, X., Wu, Y., Hao, Q., Zhang, Y., Tong, Z., Lei, W., 2020. Fluorescent MoS_2 QDs based on IFE for turn-off determination of FOX-7 in real water samples. Spectrochim. Acta A 231, 118131–118139.
Freeman, R., Finder, T., Gill, R., Willner, I., 2010. Probing protein kinase (CK2) and alkaline phosphatase with CdSe/ZnS quantum dots. Nano Lett. 10, 2192–2196.
Gan, Y., Hu, N., He, C., Zhou, S., Tu, J., Liang, T., Pan, Y., Kirsanov, D., Legin, A., Wan, H., Wang, P., 2019. MnO_2 nanosheets as the biomimetic oxidase for rapid and sensitive oxalate detection combining with bionic E-eye. Biosens. Bioelectron. 130, 254–261.
Guan, Q., Wang, G., Zhou, L., Li, W., Dong, Y., 2020. Nanoscale covalent organic frameworks as theranostic platforms for oncotherapy: synthesis, functionalization, and applications. Nanoscale Adv. 2, 3656–3733.
Han, Y., Chen, J., Li, Z., Chen, H., Qiu, H., 2020. Recent progress and prospects of alkaline phosphatase biosensor based on fluorescence strategy. Biosens. Bioelectron. 148, 111811–111822.
Hayat, A., Gonca, B., Andreescu, S., 2014. Probing phosphatase activity using redox active nanoparticles: a novel colorimetric approach for the detection of enzyme activity. Biosens. Bioelectron. 56, 334–339.
He, L., Lu, Y., Wang, F., Jing, W., Chen, Y., Liu, Y., 2018. Colorimetric sensing of silver ions based on glutathione-mediated MnO_2 nanosheets. Sens. Actuators B 254, 468–474.
Hou, X., Li, Z., Li, B., Liu, C., Xu, Z., 2018. An "off-on" fluorescein-based colormetric and fluorescent probe for the detection of glutathione and cysteine over homocysteine and its application for cell imaging. Sens. Actuators B 260, 295–302.
Hu, Q., He, M., Mei, Y., Feng, W., Jing, S., Kong, J., Zhang, X., 2017. Sensitive and selective colorimetric assay of alkaline phosphatase activity with Cu (II)-phenanthroline complex. Talanta 163, 146–152.
Hu, Q., Zhou, B., Dang, P., Li, L., Kong, J., Zhang, X., 2017. Facile colorimetric assay of alkaline phosphatase activity using Fe (II)-phenanthroline reporter. Anal. Chim. Acta 950, 170–177.
Huang, L., Cao, X., Gao, T., Feng, B., Huang, X., Song, R., Du, T., Wen, S., Feng, X., Zeng, W., 2021. A novel aggregation-induced dual emission probe for in situ light-up detection of endogenous alkaline phosphatase. Talanta 225, 121950–121957.
Ino, K., Kanno, Y., Arai, T., Inoue, K.Y., Takahashi, Y., Shiku, H., Matsue, T., 2012. Novel electrochemical methodology for activity estimation of alkaline phosphatase based on solubility difference. Anal. Chem. 84, 7593–7598.
Kim, M.I., Park, S.Y., Park, K.S., Kim, S.R., Kim, J.P., Lee, Y.C., Lee, H.U., Park, H.G., 2018. Label-free fluorescent detection of alkaline phosphatase with vegetable waste-derived green carbon probes. Sens. Actuators B 262, 469–476.
Li, C., Zou, C., Li, Y., Kong, X., Zhou, Y., Wu, Y., Zhu, W., 2013. A colormetric and fluorescent chemosensor for adenosine-5'-triphosphate based on rhodamine derivative. Anal. Chim. Acta 795, 69–74.
Liao, Y., He, G., Duan, Y., 2021. Morphology-controlled self-assembly synthesis and excellent microwave absorption performance of MnO_2 microspheres of fibrous flocculation. Chem. Eng. J. 425, 130512–130530.
Liu, Y., Cavallaro, P.M., Kim, B.M., Liu, T., Wang, H., Kuhn, F., Hodin, R.A., 2021. A role for intestinal alkaline phosphatase in preventing liver fibrosis. Theranostics 11, 14–26.
Liu, S., Han, L., Li, N., Fan, Y., Yang, Y., Li, N., Luo, H., 2019. A ratiometric fluorescent strategy for alkaline phosphatase activity assay based on g-C_3N_4/CoOOH nanohybrid via target-triggered competitive redox reaction. Sens. Actuators B 283, 515–523.
Liu, M., Jiang, K., Ding, X., Wang, S., Zhang, C., Liu, J., Zhan, Z., Cheng, G., Li, B., Chen, H., Jin, S., Tan, B., 2019. Controlling monomer feeding rate to achieve highly crystalline covalent triazine frameworks. Adv. Mater. 19, 1807865–1807872.
Liu, C., Park, E., Jin, Y., Liu, J., Yu, Y., Zhang, W., Lei, S., Hu, W., 2018. Separation of arylenevinylene macrocycles with a surface-confined two-dimensional covalent organic framework. Angew. Chem. Int. Ed. 57, 8984–8988.
Ma, J., Yin, B., Wu, X., Ye, B., 2016. Copper-mediated DNA-scaffolded silver nanocluster on-off switch for detection of pyrophosphate and alkaline phosphatase. Anal. Chem. 88, 9219–9225.
Mahdy, A.F.M., Kuo, C.H., Alshehri, A., Young, C., Yamauchi, Y., Kim, J., Kuo, S.W., 2018. Strategic design of triphenylamine- and triphenyltriazine-based two-dimensional covalent organic frameworks for CO_2 uptake and energy storage. J. Mater. Chem. A 6, 19532–19541.
Martinez Abadia, M., Stoppiello, C.T., Strutynski, K., Lerma Berlanga, B., Marti Gastaldo, C., Saeki, A., Franco, M.M., Khlobystov, A.N., Alonso, A.M., 2019. A wavy two-dimensional covalent organic framework from core-twisted polycyclic aromatic hydrocarbons. J. Am. Chem. Soc. 141, 14403–14410.
Ni, P., Chen, C., Jiang, Y., Zhang, C., Wang, B., Cao, B., Li, C., Lu, Y., 2019. Gold nanoclusters-based dual-channel assay for colorimetric and turn-on fluorescent sensing of alkaline phosphatase. Sens. Actuators B 301, 127080–127087.
Niu, X., Ye, K., Wang, L., Lin, Y., Du, D., 2019. A review on emerging principles and strategies for colorimetric and fluorescent detection of alkaline phosphatase activity. Anal. Chim. Acta 1086, 29–45.
Pachfule, P., Acharjya, A., Roeser, J., Langenhahn, T., Schwarze, M., Schomacker, R., Thomas, A., Schmidt, J., 2018. Diacetylene functionalized covalent organic framework (COF) for photocatalytic hydrogen generation. J. Am. Chem. Soc. 140, 1423–1427.
Pang, X., Li, Y., Lu, Q., Ni, Z., Zhou, Z., Xie, R., Wu, C., Li, H., Zhang, Y., 2021. A turn-on near-infrared fluorescent probe for visualization of endogenous alkaline phosphatase activity in living cells and zebrafish. Analyst 146, 521–528.
Park, C.S., Ha, T.H., Kim, M., Raja, N., Yun, H.S., Sung, M.J., Kwon, O.S., Yoon, H., Lee, C.S., 2018. Fast and sensitive near-infrared fluorescent probes for ALP detection and 3d printed calcium phosphate scaffold imaging in vivo. Biosens. Bioelectron. 105, 151–158.
Qu, Z., Yu, T., Liu, Y., Bi, L., 2021. Determination of butyrylcholinesterase activity based on thiamine luminescence modulated by MnO_2 nanosheets. Talanta 224, 121831.
Sepehri, A., Sarrafzadeh, M.H., 2018. Effect of nitrifiers community on fouling mitigation and nitrification efficiency in a membrane bioreactor. Chem. Eng. Process. 128, 10–18.
Shi, D., Sun, Y., Lin, L., Shi, C., Wang, G., Zhang, X., 2016. Naked-eye sensitive detection of alkaline phosphatase (ALP) and

pyrophosphate (PPi) based on a horseradish peroxidase catalytic colorimetric system with Cu (Ⅱ). Analyst 141, 5549–5554.
Siller, A.F., Whyte, M.P., 2018. Alkaline phosphatase: discovery and naming of our favorite enzyme. J. Bone Miner. Res. 33, 362–364.
Song, H., Wang, H., Li, X., Peng, Y., Pan, J., Niu, X., 2018. Sensitive and selective colorimetric detection of alkaline phosphatase activity based on phosphate anion-quenched oxidase-mimicking activity of Ce (IV) ions. Anal. Chim. Acta 1044, 154–161.
Stegbauer, L., Schwinghammer, K., Lotsch, B.V., 2014. A hydrazone-based covalent organic framework for photocatalytic hydrogen production. Chem. Sci. 5, 2789–2793.
Thomas, S., Li, H., Zhong, C., Matsumoto, M., Dichtel, W.R., Bredas, J.L., 2019. Electronic structure of two-dimensional π-conjugated covalent organic frameworks. Chem. Mater. 31, 3051–3065.
Wang, Y., Jiang, K., Zhu, J., Zhang, L., Lin, H., 2015. A FRET-based carbon dot-MnO_2 nanosheet architecture for glutathione sensing in human whole blood samples. Chem. Commun. 51, 12748–12751.
Wu, C., Hu, X., Gu, B., Yin, P., Su, W., Li, Y., Lu, Q., Zhang, Y., Li, H., 2018. A lysosome-targeting colorimetric and fluorescent dual signal probe for sensitive detection and bioimaging of hydrogen sulfide. Anal. Methods 10, 604–610.
Xiao, T., Sun, J., Zhao, J., Wang, S., Liu, G., Yang, X., 2018. FRET effect between fluorescent polydopamine nanoparticles and MnO_2 nanosheets and its application for sensitive sensing of alkaline phosphatase. ACS Appl. Mater. Interfaces 10, 6560–6569.
Xu, H., Gao, J., Jiang, D., 2015. Stable, crystalline, porous, covalent organic frameworks as a platform for chiral organocatalysts. Nat. Chem. 7, 905–912.
Yan, X., Song, Y., Wu, X., Zhu, C., Su, X., Du, D., Lin, Y., 2017. Oxidase-mimicking activity of ultrathin MnO_2 nanosheets in colorimetric assay of acetylcholinesterase activity. Nanoscale 9, 2317–2323.
Yan, G., Zhang, Y., Di, W., 2018. An enzymatic reaction mediated glucose sensor activated by MnO_2 nanosheets acting as an oxidant and catalyst. Analyst 143, 2915–2922.
Yang, Q., Li, C., Li, J., Arabi, M., Wang, X., Peng, H., Xiong, H., Choo, J., Chen, L., 2020. Multi-emitting fluorescence sensor of MnO_2-OPD-QD for the multiplex and visual detection of ascorbic acid and alkaline phosphatase. J. Mater. Chem. C 8, 5554–5561.
Yang, Q., Wang, X., Peng, H., Arabi, M., Li, J., Xiong, H., Choo, J., Chen, L., 2020. Ratiometric fluorescence and colorimetry dual-mode assay based on manganese dioxide nanosheets for visual detection of alkaline phosphatase activity. Sens. Actuators B 302, 127176–127186.
Yang, J., Zheng, L., Wang, Y., Li, W., Zhang, J., Gu, J., Fu, Y., 2016. Guanine-rich DNA-based peroxidase mimetics for colorimetric assays of alkaline phosphatase. Biosens. Bioelectron. 77, 549–556.
Ye, K., Wang, L., Song, H., Li, X., Niu, X., 2019. Bifunctional MIL-53(Fe) with pyrophosphate-mediated peroxidase-like activity and oxidation-stimulated fluorescence switching for alkaline phosphatase detection. J. Mater. Chem. B 7, 4794–4800.
Zhang, J., Han, X., Wu, X., Liu, Y., Cui, Y., 2017. Multivariate chiral covalent organic frameworks with controlled crystallinity and stability for asymmetric catalysis. J. Am. Chem. Soc. 139, 8277–8285.
Zhang, J., Chen, R., Chen, Q., Hu, Y., Pan, S., Hu, X., 2021. Ratiometric fluorescent probe for ascorbic acid detection based on MnO_2 nanosheets, gold nanoclusters and thiamine. Colloid Surface A 622, 126605–126613.
Zhang, Y., Wu, Y., Liu, L., Wang, W., Zhang, W., Song, D., Wang, X., Su, R., 2021. A dual-signal sensing platform based on nanosheet materials for ratiometric fluorescence and colorimetric detection of enzyme activities in human blood. Sens. Actuators B 346, 130531–130541.
Zhang, C., Zhang, S., Yan, Y., Xia, F., Huang, A., Xian, Y., 2017. Highly fluorescent polyimide covalent organic nanosheets as sensing probes for the detection of 2,4,6-trinitrophenol. ACS Appl. Mater. Interfaces 9, 13415–13421.
Zhi, Y., Li, Z., Feng, X., Xia, H., Zhang, Y., Shi, Z., Mu, Y., Liu, X., 2017. Covalent organic frameworks as metal-free heterogeneous photocatalysts for organic transformations. J. Mater. Chem. A 5, 22933–22938.